Angle-resolved x-ray photoelectron spectroscopy study of GeO_x growth by plasma post-oxidation*

Zhiqian Zhao(赵治乾)[1], Jing Zhang(张静)[1,†], Xiaolei Wang(王晓磊)[2,3,‡], Shuhua Wei(魏淑华)[1], Chao Zhao(赵超)[2,3], and Wenwu Wang(王文武)[2,3]

[1] *Microelectronics Department, North China University of Technology, Beijing* 100041, *China*
[2] *Key Laboratory of Microelectronics Devices & Integrated Technology, Institute of Microelectronics, Chinese Academy of Sciences, Beijing* 100029, *China*
[3] *School of Microelectronics, University of Chinese Academy of Sciences, Beijing* 100049, *China*

(Received 1 April 2017; revised manuscript received 15 June 2017; published online 20 August 2017)

The growth process of GeO_x films formed by plasma post-oxidation (PPO) at room temperature (RT) is investigated using angle-resolved x-ray photoelectron spectroscopy (AR-XPS). The experimental results show that the distributions of the Ge^{4+} states, a mixture of the Ge^{2+} and Ge^{3+} states, and the Ge^{1+} states are localized from the GeO_x surface to the GeO_x/Ge interface. Moreover, the Ge^{1+} states are predominant when the two outermost layers of Ge atoms are oxidized. These findings are helpful for establishing in-depth knowledge of the growth mechanism of the GeO_x layer and valuable for the optimization of Ge-based gate stacks for future complementary metal–oxide–semiconductor (MOS) field-effect transistor (CMOSFET) devices.

Keywords: Ge, plasma post-oxidation, MOS, XPS

PACS: 82.80.Pv, 81.65.Mq, 52.77.Dq **DOI:** 10.1088/1674-1056/26/10/108201

1. Introduction

As Si transistor technology advances beyond the 10-nm node, it has been more difficult to further enhance the performance of MOSFETs on the Si platform owing to the inherent limitations of the Si material itself. The device research community is increasingly paying close attention to the replacement of Si in the transistor channel with novel and high-mobility materials.[1,2] Among several possible candidate materials, Ge is a promising material that can offer increases in the electron and hole mobilities by factors of approximately two and four, respectively, compared with those of Si and can provide compatibility with conventional Si integration technologies.[1,3,4] However, several issues still need to be resolved before Ge can be completely applied to field-effect transistors (FETs) as a proven technology to attain a high performance. One of the critical issues is to provide a high-quality interfacial layer, which can avoid causing a substantial degradation in the drive current in both the low equivalent oxide thickness (EOT) and short-channel regimes.[3]

Recently, wide ranges of materials and processes have been researched to achieve superior Ge surface passivation, including nitride,[5–11] Si,[12–15] S,[16–20] and Ge dioxide or suboxide (GeO_x)[20–38] passivation layers. High-quality GeO_2 has recently been reconsidered as a promising passivation layer owing to its extremely low D_{it} ($\sim 6\times10^{10}$ $eV^{-1}\cdot cm^{-2}$)[39] and its potential to enable high-performance Ge n-MOSFETs.[40] GeO_2 or GeO_x can be grown by thermal oxidation at atmospheric pressure[21,22] and high pressure ($\sim$ 70 atm; 1 atm = 1.01325×10^5 Pa),[23,24] respectively, as well as plasma post-oxidation (PPO)[33–38,41–46] or ozone oxidation.[29–32] Lee *et al.*[24] proposed a two-step oxidation process with high-pressure (70 atm) oxidation and low-temperature oxygen annealing to form an ideal GeO_2/Ge stack based on thermodynamic and kinetic control. A GeO_2 thickness of about 20 nm and $D_{it} < 10^{11}$ $eV^{-1}\cdot cm^{-2}$ near the midgap were obtained with a peak electron mobility of 1100 $cm^2\cdot V^{-1}\cdot s^{-1}$. Kuzum *et al.*[30] used ozone oxidation to grow GeO_x and achieved a mobility that is $\sim$ 1.5 times higher than the universal Si mobility. Zhang *et al.*[37] demonstrated that by using the electron cyclotron resonance oxygen PPO method, the EOT of the $HfO_2/Al_2O_3/GeO_x$/Ge gate stack can be scaled down to 0.7 nm–0.8 nm while maintaining D_{it} at a level of 10^{11} $eV^{-1}\cdot cm^{-2}$. Further, the peak electron and hole mobilities were 689 $cm^2\cdot V^{-1}\cdot s^{-1}$ and 546 $cm^2\cdot V^{-1}\cdot s^{-1}$, respectively.

In order to further improve the interfacial properties using PPO, it is necessary to understand the distributions of various Ge oxidation states in the GeO_x interfacial layer. In this paper, the areal intensity ratios of these oxidation states in a GeO_x interfacial layer formed by PPO technology are investigated using angle-resolved x-ray photoelectron spectroscopy (AR-XPS). Moreover, the distributions of the Ge oxidation states

*Project supported by the National Natural Science Foundation of China (Grant Nos. 61574168 and 61504163).
†Corresponding author. E-mail: zhangj@ncut.edu.cn
‡Corresponding author. E-mail: wangxiaolei@ime.ac.cn
© 2017 Chinese Physical Society and IOP Publishing Ltd

are obtained by these areal intensity ratios.

2. Experimental

In order to fabricate the GeO_x/Ge interface, an HF-last process (100:1 H_2O:HF for 2 min) was carried out to remove the native Ge oxide on a Ge (100) wafer. Subsequently, the wafers were immediately capped with a 3-nm-thick Al_2O_3 layer by atomic layer deposition (ALD) at a substrate temperature of 300 °C with $Al(CH_3)_3$ (trimethylaluminum, TMA) and H_2O as precursors. Finally, the Al_2O_3/GeO_x/Ge structure was fabricated at room temperature (RT; ∼ 20 °C) by PPO. The inductively coupled plasma (ICP) was made up of an Ar (650 sccm) and O_2 (50 sccm) gas mixture, and the microwave power was 96 W. The bias voltage between the plasma source and the samples was less than 1 V. AR-XPS (Thermo Scientific ESCALAB 250xi) was performed with a monochromatic Al Kα radiation source. All high-resolution spectra were obtained with a pass energy of 15 eV. The takeoff angle was 90° when the photoelectron emission direction was normal to the sample surface.

The thickness of GeO_x interface layer was controlled by regulating the time of post plasma oxidation, and the thickness of GeO_x interface layer was calculated as follows. According to the theory of x-ray photoelectron spectroscopy that the intensity attenuation of photoelectron with characteristic energy obeys the exponential distribution, if each layer of atoms emits a photoelectron intensity I_0 toward the surface, then the measured intensity of electrons (I') of a given layer arriving at the surface layer will be

$$I' = I_0 \cdot \exp\left(-\frac{t}{\lambda_{E_k} \cdot \sin\theta}\right), \tag{1}$$

where t is the distance of that layer from the surface, λ_{E_k} is the photoelectron mean free path, and θ is the angle between the horizontal surface and the emitting light. Since the core electrons are tightly bound, it is rational to assume that the photoelectron intensity I_0 originating from the plane of each layer is the same. All the measured intensity of photoelectron (I) originating from the surface to the given layer would be obtained by integrating Eq. (1) from 0 to t,

$$I = -I_0 \cdot \lambda_{E_k} \cdot \sin\theta \cdot \left(\exp\left(-\frac{t}{\lambda_{E_k} \cdot \sin\theta}\right) - 1\right). \tag{2}$$

Equation (2) corresponds to the case of a single material sample. If other materials (A) are stacked above the material to be tested (B), the measured intensity of photoelectron (I) originated from overall material (B) will be

$$I = -I_0 \cdot \lambda_{E_{kB}} \cdot \sin\theta \cdot \left(\exp\left(-\frac{t_B}{\lambda_{E_{kB}} \cdot \sin\theta}\right) - 1\right) \times \exp\left(-\frac{t_A}{\lambda_{E_{kA}} \cdot \sin\theta}\right). \tag{3}$$

The gate-stack structure of the sample is shown in Fig. 1.

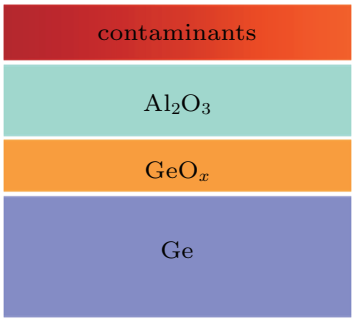


Fig. 1. (color online) The gate-stack structure of the sample.

On the basis of the above discussion, the equations of measured intensity of Ge and GeO_x are shown as follows:

$$I_{\mathrm{Ge}}(\theta) = -I_{0\,\mathrm{Ge}} \cdot \lambda^{\mathrm{Ge}}_{\mathrm{Ge_{3d}}} \cdot \sin\theta \cdot \left(\exp\left(-\frac{\infty}{\lambda^{\mathrm{Ge}}_{\mathrm{Ge_{3d}}} \cdot \sin\theta}\right) - 1\right) \times \sin\theta \cdot \exp\left(-\frac{d_{\mathrm{GeO}_x}}{\lambda^{\mathrm{GeO}_x}_{\mathrm{Ge_{3d}}} \cdot \sin\theta}\right) \times \exp\left(-\frac{d_{\mathrm{Al_2O_3}}}{\lambda^{\mathrm{Al_2O_3}}_{\mathrm{Ge_{3d}}} \cdot \sin\theta}\right) \times \exp\left(-\frac{d_{\mathrm{contaminants}}}{\lambda^{\mathrm{contaminants}}_{\mathrm{Ge_{3d}}} \cdot \sin\theta}\right), \tag{4}$$

$$I_{\mathrm{GeO}_x}(\theta) = -I_{0\,\mathrm{GeO}_x} \cdot \lambda^{\mathrm{GeO}_x}_{\mathrm{Ge_{3d}}} \cdot \sin\theta \times \left(\exp\left(-\frac{d_{\mathrm{GeO}_x}}{\lambda^{\mathrm{GeO}_x}_{\mathrm{Ge_{3d}}} \cdot \sin\theta}\right) - 1\right) \times \sin\theta \cdot \exp\left(-\frac{d_{\mathrm{Al_2O_3}}}{\lambda^{\mathrm{Al_2O_3}}_{\mathrm{Ge_{3d}}} \cdot \sin\theta}\right) \times \exp\left(-\frac{d_{\mathrm{contaminants}}}{\lambda^{\mathrm{contaminants}}_{\mathrm{Ge_{3d}}} \cdot \sin\theta}\right), \tag{5}$$

$$\frac{I_{\mathrm{GeO}_x}(\theta)}{I_{\mathrm{Ge}}(\theta)} = \frac{\lambda^{\mathrm{GeO}_x}_{\mathrm{Ge_{3d}}}}{\lambda^{\mathrm{Ge}}_{\mathrm{Ge_{3d}}}} \cdot \frac{\rho_{\mathrm{GeO}_x}}{\rho_{\mathrm{Ge}}} \cdot \left(\exp\left(\frac{d_{\mathrm{GeO}_x}}{\lambda^{\mathrm{GeO}_x}_{\mathrm{Ge_{3d}}} \cdot \sin\theta}\right) - 1\right). \tag{6}$$

Here $I_{\mathrm{GeO}_x}(\theta)$ and $I_{\mathrm{Ge}}(\theta)$ is the areal intensity of GeO_x and Ge, respectively, which is measured at the takeoff angle of θ. ρ_{GeO_x} and ρ_{Ge} is the germanium-atomic-density of GeO_x and Ge of each atomic layer, respectively. $d_{\mathrm{contaminants}}$, $d_{\mathrm{Al_2O_3}}$, and d_{GeO_x} are the thicknesses of contaminants, Al_2O_3, and GeO_x, respectively. $\lambda^{\mathrm{GeO}_x}_{\mathrm{Ge_{3d}}}$, $\lambda^{\mathrm{Ge}}_{\mathrm{Ge_{3d}}}$, $\lambda^{\mathrm{Al_2O_3}}_{\mathrm{Ge_{3d}}}$, and $\lambda^{\mathrm{contaminants}}_{\mathrm{Ge_{3d}}}$ are the inelastic mean free path of photoelectrons of Ge 3d in GeO_x, Ge, Al_2O_3, and contaminants, respectively. The items about Al_2O_3, contaminants, and any other material layer located upon the GeO_x and Ge layers can be eliminated by dividing Eq. (4) from Eq. (5), because the intensity attenuation of Ge 3d of GeO_x and Ge from such layers are the same. Then, the thickness of GeO_x interface layer can be calculated by Eq. (6).

The $\lambda_{Ge_{3d}}^{GeO_x}$ and $\lambda_{Ge_{3d}}^{Ge}$ are taken as 2.48 nm and 2.64 nm, respectively. The ρ_{GeO_x} and ρ_{Ge} are taken as 2.53×10^{22} cm^{-3} and 4.42×10^{22} cm^{-3}.[47]

3. Results and discussion

In order to investigate the oxidation states and their distributions in the GeO_x interfacial layer formed by PPO, the XPS spectra of the Ge 3d core level were recorded and analyzed. Figure 2 shows the Ge 3d XPS spectra for $Al_2O_3/GeO_x/Ge$ structures with different GeO_x thicknesses at a takeoff angle of 90°. In order to quantitatively estimate the various states of the Ge components, the Ge 3d spectra were deconvoluted into five peaks related to the Ge substrate (Ge^0), Ge suboxide (Ge^{1+}, Ge^{2+}, and Ge^{3+}), and GeO_2 (Ge^{4+}), as shown in Fig. 2. Further, the chemical shifts of Ge^{1+}, Ge^{2+}, Ge^{3+}, and Ge^{4+} relative to Ge^0 are taken as 0.8, 1.8, 2.75, and 3.4 eV, respectively.[48–52] A spin–orbit splitting of 0.585 eV and a branching ratio of 2:3 are used for the $3d_{5/2}$ and Ge $3d_{3/2}$ doublets of the Ge 3d line shape. The Shirley background is used. The full width at half maximum (FWHM) is 0.57 eV for Ge^0 and Ge^{1+}, 0.9 eV for Ge^{2+}, 1.12 eV for Ge^{3+}, and 1.2 eV for Ge^{4+}.[52] In addition, the symmetric Lorentzian–Gaussian convolution function is used, and the optimized percentage of the Lorentzian–Gaussian function is found to be 20%.

To obtain a better understanding of the oxidation process, it is necessary to clarify the depth distributions of the various oxidation states of Ge. Figure 3 shows the areal intensity ratios of the various states of Ge components as a function of the takeoff angle for a GeO_x thickness of 0.59 nm after deconvolution of the spectra in Fig. 1. Considering that the spectra obtained with smaller takeoff angle are more sensitive to the surface, the photoelectrons received at a takeoff angle of 35° more often originate from the Ge atoms in the surface layer compared to those received at 90°. Therefore, the results measured at 35° are more likely to reflect the surface elements, whereas those measured at 90° reflect the elements in the entire sample.

It can be clearly observed from Fig. 3(a) that Ge^{x+}/Ge^0 ($x = 1, 2, 3, 4$) decreases with increasing takeoff angle, suggesting that all oxidation states are located above the Ge^0 states. A similar phenomenon is observed in Figs. 3(b), 3(c), and 3(d), indicating that the Ge^{x+} ($x = 2, 3, 4$) states are located above the Ge^{1+} states, and the Ge^{4+} states appear above the Ge^{2+} and Ge^{3+} states. In contrast, the ratio of Ge^{3+}/Ge^{2+} in Fig. 3(c) increases with increasing takeoff angle, demonstrating that the Ge^{2+} states are located above the Ge^{3+} states. On the basis of the above discussion, the distributions of the various oxidation states of Ge in 0.59-nm-thick GeO_x are obtained as follows. The Ge^{4+}, Ge^{2+}, Ge^{3+}, and Ge^{1+} states are localized from the GeO_x surface to the GeO_x/Ge interface but not in the order of Ge^{4+}, Ge^{3+}, Ge^{2+}, and Ge^{1+} predicted by the layer-by-layer growth mode.[38]

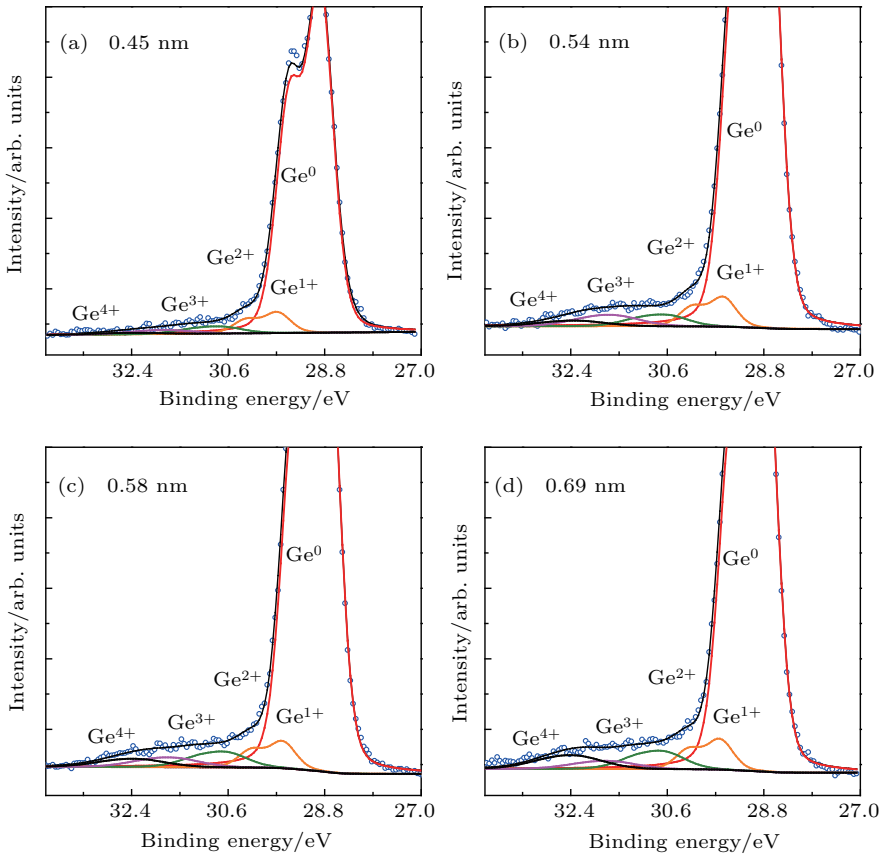


Fig. 2. (color online) Ge 3d XPS spectra for $Al_2O_3/GeO_x/Ge$ structures with different GeO_x thicknesses at a takeoff angle of 90°. The Ge 3d spectra consist of five peaks related to the Ge substrate (Ge^0), Ge suboxide (Ge^{1+}, Ge^{2+}, Ge^{3+}), and GeO_2 (Ge^{4+}). The spin–orbit splitting of the Ge $3d_{5/2}$ and Ge $3d_{3/2}$ doublets is 0.585 eV.

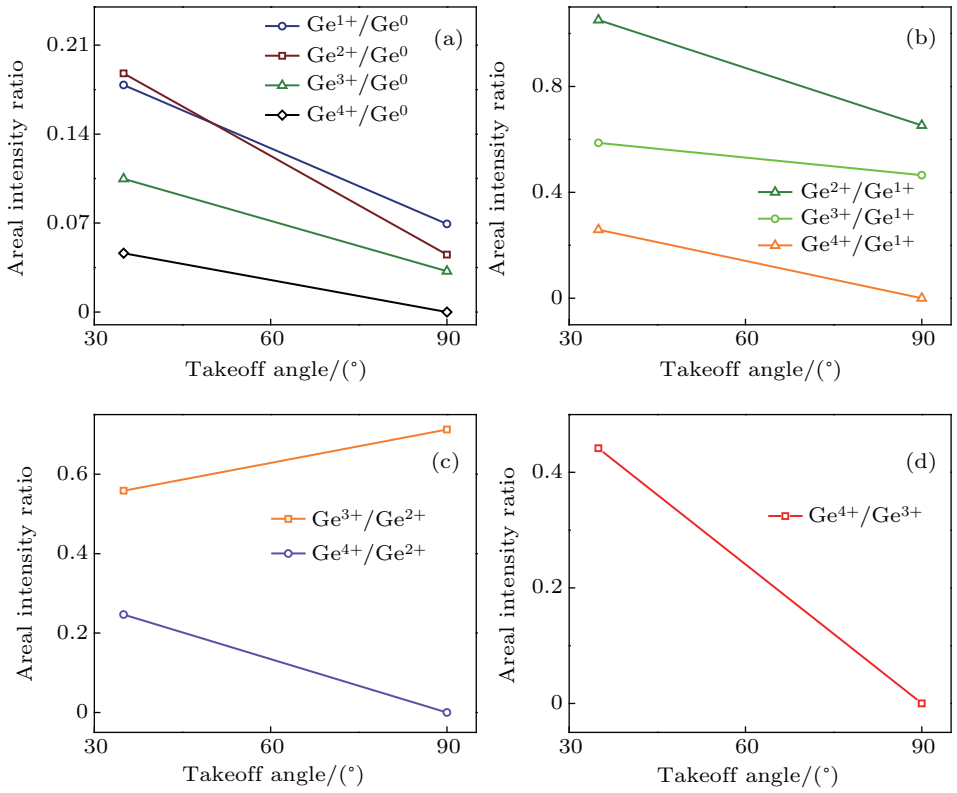


Fig. 3. (color online) Areal intensity ratios of various states of Ge components as a function of the takeoff angle for a GeO_x thickness of 0.59 nm. According to these results, the depth distributions of the Ge oxidation states are obtained.

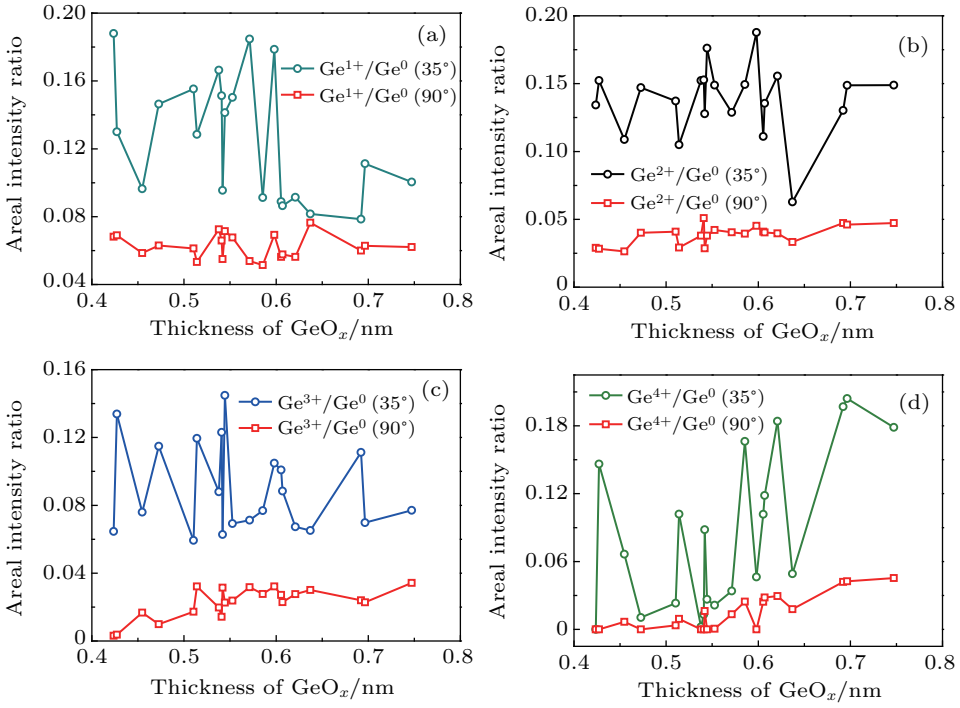


Fig. 4. (color online) Areal intensity ratios of Ge^{x+}/Ge^0 ($x = 1, 2, 3, 4$) as a function of the GeO_x thickness for takeoff angles of 35° and 90°. The relationship between the distributions of the Ge^{x+} and Ge^0 states can be acquired from these results.

For a more objective understanding of the distributions of the Ge oxidation states during the oxidation process, the areal intensity ratios of various Ge oxidation states as a function of the GeO_x thickness for takeoff angles of 35° and 90° have been investigated, as shown in Figs. 4, 5, and 6.

It can be clearly observed from Fig. 4 that the values of Ge^{x+}/Ge^0 ($x = 1, 2, 3, 4$) at a takeoff angle of 35° are higher than those at 90° for GeO_x thicknesses of 0.42–0.75 nm, suggesting that all Ge oxidation states are located above the Ge^0 states. A similar phenomenon is observed for the results in

Fig. 5, indicating that the Ge^{x+} ($x = 2, 3, 4$) states are located above the Ge^{1+} states, and the Ge^{4+} states are located above the Ge^{3+} states. Figure 6 shows Ge^{3+}/Ge^{2+} and Ge^{4+}/Ge^{2+} as a function of the GeO_x thickness. For Ge^{3+}/Ge^{2+} in Fig. 6(a), Ge^{3+}/Ge^{2+} for a takeoff angle of 90° is larger than that for 35° for some GeO_x thicknesses and smaller for other GeO_x thicknesses. These results indicate that the Ge^{2+} states appear above the Ge^{3+} states for some GeO_x thicknesses and below the Ge^{3+} states for other GeO_x thicknesses. Figure 6(b) shows Ge^{4+}/Ge^{2+} as a function of the GeO_x thickness. The Ge^{4+} states are located above the Ge^{2+} states. According to the discussion above, the distribution of the Ge oxidation states of the GeO_x interfacial layer during the oxidation process are obtained as follows. The Ge^{4+} states, a mixture of Ge^{2+} and Ge^{3+} states, and the Ge^{1+} states are localized from the GeO_x surface to the GeO_x/Ge interface.

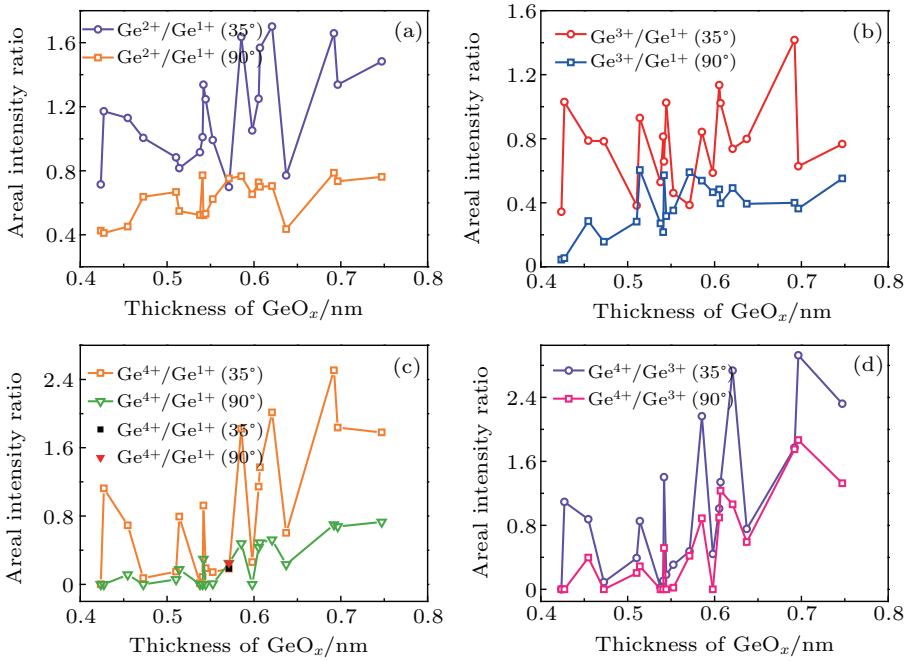


Fig. 5. (color online) Areal intensity ratios of Ge^{x+}/Ge^{1+} ($x = 2, 3, 4$) and Ge^{4+}/Ge^{3+} as a function of the GeO_x thickness for takeoff angles of 35° and 90°.

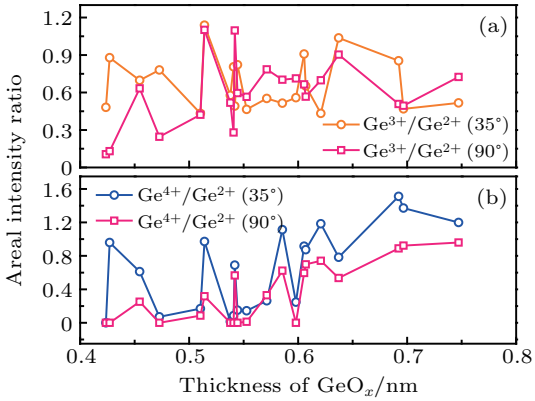


Fig. 6. (color online) Areal intensity ratios of Ge^{3+}/Ge^{2+} and Ge^{4+}/Ge^{2+} as a function of the GeO_x thickness for takeoff angles of 35° and 90°.

Figure 7 shows the areal intensity ratios of Ge^{x+}/Ge^{1+} ($x = 3, 4$) and $(Ge^{3+}+Ge^{4+})/Ge^{1+}$ as a function of the GeO_x thickness for a takeoff angle of 90°. It can be clearly observed that almost all areal intensity ratios (except for three) were less than 1.0, indicating that the number of Ge^{1+} states existing in a GeO_x layer with a thickness of 1 nm or less is far greater than the numbers of Ge^{3+} and Ge^{4+} states and even greater than their sum. The Ge–Ge distance in GeO_2 is in the range of 3.05 Å–3.15 Å,[53] which means that two layers of Ge should be oxidized for 0.7-nm-thick GeO_x. Consequently, the Ge^{1+} states are predominant when the two outermost layers of Ge atoms are oxidized.

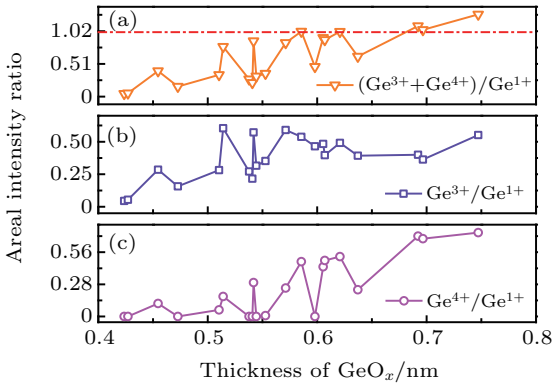


Fig. 7. (color online) Areal intensity ratios of Ge^{x+}/Ge^{1+} ($x = 3, 4$) and $(Ge^{3+}+Ge^{4+})/Ge^{1+}$ as a function of the GeO_x thickness for a takeoff angle of 90°.

4. Conclusions

In summary, the growth process of a GeO_x film formed by PPO at RT is investigated on the basis of AR-XPS. In addition,

the distributions of various Ge oxidation states are obtained by the areal intensity ratios of these states. It is experimentally found that the distributions of the Ge^{4+} states, a mixture of the Ge^{2+} and Ge^{3+} states, and the Ge^{1+} states are localized from the GeO_x surface to the GeO_x/Ge interface. Furthermore, the Ge^{1+} states are predominant when the two outermost layers of Ge atoms are oxidized. These experimental results are helpful for optimizing Ge-based gate stacks for future CMOSFET devices.

Acknowledgments

We would like to thank Editage (www.editage.com) for English language editing.

References

[1] Gupta S, Gong X, Zhang R, Yeo Y C, Takagi S and Saraswat K C 2014 *MRS Bull.* **39** 678
[2] Takagi S 2011 *IEEE Int. Electron Devices Meeting*, Short course
[3] Xie Q, Deng S, Schaekers M, Lin D, Caymax M, Delabie A, Qu X P, Jiang Y L, Deduytsche D and Detavernier C 2012 *Semicond. Sci. Technol.* **27** 074012
[4] Saraswat K C, Chui C O, Krishnamohan T, Nayfeh A and McIntyre P 2005 *Microelectron. Eng.* **80** 15
[5] Otani Y, Itayama Y, Tanaka T, Fukuda Y, Toyota H, Ono T, Mitsui M and Nakagawa K 2007 *Appl. Phys. Lett.* **90** 142114
[6] Maeda T, Nishizawa M, Morita Y and Takagi S 2007 *Appl. Phys. Lett.* **90** 072911
[7] Bera M K, Mahata C, Chakraborty A K, Nandi S K, Tiwari J N, Hung J Y and Maiti C K 2007 *Semicond. Sci. Technol.* **22** 1352
[8] Sugawara T, Oshima Y, Sreenivasan R and McIntyre P C 2007 *Appl. Phys. Lett.* **90** 112912
[9] Ritenour A, Hennessy J and Antoniadis D A 2007 *IEEE Electron Dev. Lett.* **28** 746
[10] Kim K H, Gordon R G, Ritenour A and Antoniadis D A 2007 *Appl. Phys. Lett.* **90** 212104.
[11] Xie R, Phung T H, Yu M and Zhu C 2010 *IEEE Trans. Electron Dev.* **57** 1399
[12] Wu N, Zhang Q, Zhu C, Chan D S H, Li M F, Balasubramanian N, Chin A and Kwong D L 2004 *Appl. Phys. Lett.* **85** 4127
[13] Wu N, Zhang Q, Zhu C, Chan D S H, Du A, Balasubramanian N, Li M F, Sin J K O and Kwong D L 2004 *IEEE Electron Dev. Lett.* **25** 631
[14] Caymax M, Leys F, Mitard J, Martens K, Yang L, Pourtois G, Vandervorst W, Meuris M and Loo R 2009 *J. Electrochem. Soc.* **156** H979
[15] Chen W B, Shie B S and Chin A 2011 *IEEE Electron Dev. Lett.* **32** 449
[16] Frank M M, Koester S J, Copel M, Ott J A and Loesing R 2006 *Appl. Phys. Lett.* **89** 112905
[17] Xie R and Zhu C 2007 *IEEE Electron Dev. Lett.* **28** 976
[18] Sioncke S, Lin H C, Brammertz G, Delabie A, Conard T, Franquet A, Meuris M, Struyf H, Gendt S De, Heyns M, Fleischmann C, Temst K, Vantomme A, Müller M, Kolbe M, Beckhoff B and Caymax M 2011 *J. Electrochem. Soc.* **158** H687
[19] Merckling C, Chang Y C, Lu C Y, Penaud J, El-Kazzi M, Bellenger F, Brammertz G, Hong M, Kwo J, Meuris M, Dekoster J, Heyns M M and Caymax M 2011 *Microelectron. Eng.* **88** 399
[20] Matsubara H, Sasada T, Takenaka M and Takagi S 2008 *Appl. Phys. Lett.* **93** 032104
[21] Hosoi T, Kutsuki K, Okamoto G, Saito M, Shimura T and Watanabe H 2009 *Appl. Phys. Lett.* **94** 202112
[22] Lee C H, Tabata T, Nishimura T, Nagashio K, Kita K and Toriumi A 2009 *Appl. Phys. Express* **2** 071404
[23] Lee C H, Nishimura T, Nagashio K, Kita K and Toriumi A 2011 *IEEE Trans. Electron Dev.* **58** 1295
[24] Delabie A, Bellenger F, Houssa M, Conard T, Elshocht S V, Caymax M, Heyns M and Meuris M 2007 *Appl. Phys. Lett.* **91** 082904
[25] Matsubara H, Sasada T, Takenaka M and Takagi S 2008 *Appl. Phys. Lett.* **93** 032104
[26] Xie R, He W, Yu M and Zhu C 2008 *Appl. Phys. Lett.* **93** 073504
[27] Gu J J, Liu Y Q, Xu M, Celler G K, Gordon R G and Ye P D 2010 *Appl. Phys. Lett.* **97** 012106
[28] Delabie A, Alian A, Bellenger F, Caymax M, Conard T, Franquet A, Sioncke S, Van Elshocht S, Heyns M M and Meuris M 2009 *J. Electrochem. Soc.* **156** G163
[29] Kuzum D, Krishnamohan T, Pethe A J, Okyay A K, Oshima Y, Sun Y, McVittie J P, Pianetta P A, McIntyre P C and Saraswat K C 2008 *IEEE Electron Dev. Lett.* **29** 328
[30] Yang X, Wang S K, Zhang X, Sun B, Zhao W, Chang H D, Zeng Z H and Liu H 2014 *Appl. Phys. Lett* **105** 092101
[31] Wang X L, Xiang J J, Wang W W, Xiong Y H, Zhang J and Zhao C 2015 *Appl. Surf. Sci.* **357** 1857
[32] Fukuda Y, Yazaki Y, Otani Y, Sato T, Toyota H and Ono T 2010 *IEEE Trans. Electron Dev.* **57** 282
[33] Zhang R, Iwasaki T, Taoka N, Takenaka M and Takagi S 2012 *IEEE Trans. Electron Dev.* **59** 335
[34] Takenaka M, Zhang R and Takagi S 2013 *Reliability Physics Symposium* (IRPS) 4C.1.1–4C.1.8
[35] Takagi S, Zhang R and Takenaka M 2013 *Microelectron. Eng.* **109** 389
[36] Zhang R, Lin J C, Yu X, Takenaka M and Takagi S 2013 *Microelectron. Eng.* **109** 97
[37] Zhang R, Huang P C, Lin J C, Takenaka M and Takagi S 2013 *Appl. Phys. Lett.* **102** 081603
[38] Zhang R, Huang P C, Lin J C, Taoka N, Takenaka M and Takagi S 2013 *IEEE Trans. Electron Dev.* **60** 927
[39] Takahashi T, Nishimura T, Chen L, Sakata S, Kita K and Toriumi A 2007 *IEEE Int. Electron Devices Meeting*, p. 697
[40] Hattori T and Suzuki T 1983 *Appl. Phys. Lett.* **43** 470
[41] Zhang R, Chern W, Yu X, Takenaka M, Hoyt J L and Takagi S 2013 *IEEE Int. Electron Devices Meeting*, 26.1.1–26.1.4
[42] Zhang R, Lin J C, Yu X, Takenaka M and Takagi S 2013 *Symp. VLSI Technology*, pp. T26–T27
[43] Zhang R, Huang P C, Lin J C, Takenaka M and Takagi S 2012 *IEEE Int. Electron Devices Meeting*, pp. 371–374
[44] Hosoi T, Kutsuki K, Okamoto G, Saito M, Shimura T and Watanabe H 2009 *Appl. Phys. Lett.* **94** 202112
[45] Ogawa S, Suda T, Yamamoto T, Kutsuki K, Hideshima I, Hosoi T, Shimura T and Watanabe H 2011 *Appl. Phys. Lett.* **99** 142101
[46] Fukuda Y, Ueno T, Hirono S and Hashimoto S 2005 *Jpn. J. Appl. Phys.* **44** 6981
[47] Kimihiko K, Kyogoku S, Sakashita M, Takeuchi W, Kondo H, Takeuchi S, Nakatsuka O and Zaima S 2011 *Jpn. J. Appl. Phys.* **50** 10PE02
[48] Sun S, Sun Y, Liu Z, Lee D I and Pianetta P 2006 *Appl. Phys. Lett.* **89** 231925
[49] Renault O, Fourdrinier L, Martinez E, Clavelier L, Leroyer C, Barrett N and Crotti C 2007 *Appl. Phys. Lett.* **90** 052112
[50] Kato K, Kyogoku S, Sakashita M, Takeuchi W, Kondo H, Takeuchi S, Nakatsuka O and Zaima S 2011 *Jpn. J. Appl. Phys.* **50** 10PE02
[51] Sahari S K, Murakami H, Fujioka T, Bando T, Ohta A, Makihara K, Higashi S and Miyazaki S 2011 *J. Appl. Phys.* **50** 04DA12
[52] Wang X L, Zhao Z Q, Xiang J J, Wang W W, Zhang J, Zhao C and Ye T C 2016 *Appl. Surf. Sci.* **390** 472
[53] Glinnemann J, King H E Jr, Schulz H, Hahn Th, La Placa S J and Dacol F 1992 *Z. Kristall. – Cryst. Mater.* **198** 177